Physics of Plasmas ARTICLE scitation.org/journal/php

Whistler wave generation by electron temperature anisotropy during magnetic reconnection at the magnetopause

Cite as: Phys. Plasmas **26**, 052902 (2019); doi: 10.1063/1.5094636
Submitted: 4 March 2019 · Accepted: 1 May 2019 ·
Published Online: 23 May 2019

View Online Export Citation CrossMark

Jongsoo Yoo,[1,a),b)] Shan Wang,[2] Evan Yerger,[1] J. Jara-Almonte,[1] Hantao Ji,[1] Masaaki Yamada,[1] Li-Jen Chen,[2] William Fox,[1] Aaron Goodman,[1] and Andrew Alt[1]

AFFILIATIONS

[1]Princeton Plasma Physics Laboratory, Princeton, New Jersey 08543, USA
[2]NASA Goddard Space Flight Center, Greenbelt, Maryland 20771, USA

Note: This paper is part of the Special Collection: Papers from the 60th Annual Meeting of the APS Division of Plasma Physics.
Note: Paper UI2 3 Bull. Am. Phys. Soc. **63** (2018).
[a)]Invited speaker.
[b)]**Electronic mail:** jyoo@pppl.gov

ABSTRACT

Two magnetopause reconnection events of the Magnetospheric Multiscale mission with whistler wave activity are presented. The whistler mode around half of the electron cyclotron frequency is excited near the magnetospheric separatrix. In both events, there are positive correlations between the whistler wave and the lower hybrid drift instability (LHDI) activities, indicating a possible role of LHDI in the whistler wave generation. A sudden change in the electron pitch angle distribution (PAD) function of energetic electrons is observed right after intense LHDI activity. This change in the PAD leads to temperature anisotropy in energetic electrons which is responsible for the whistler wave excitation. The measured dispersion relation demonstrates that the whistler wave propagates toward the X line nearly parallel to the magnetic field line. Finally, a linear analysis with the measured distribution function verifies that the whistler mode is excited by the temperature anisotropy in energetic electrons.

I. INTRODUCTION

Magnetic reconnection, a topological rearrangement of magnetic field lines, plays an important role in explosive phenomena in magnetized plasmas such as solar flares and substorms.[1,2] Magnetic reconnection converts magnetic energy efficiently to plasma particles, and the reconnection site has many free energy sources for waves.[3] The waves generated by free energy sources potentially impact reconnection dynamics via wave particle interactions.

Observations of waves in space have been increasing since NASA's Magnetospheric Multiscale (MMS) was launched in 2014. The unprecedented temporal resolution in both particle and field measurements has provided opportunities for studying waves quantitatively in space. In particular, whistler waves have been widely observed near the magnetospheric separatrix[4–7] as well as near the electron diffusion region[8] during asymmetric reconnection at the dayside magnetopause.

Recently, Yoo *et al.*[7] have demonstrated that whistler waves near the magnetospheric separatrix are excited by temperature anisotropy in tail electrons and propagate toward the X line mostly parallel to the background magnetic field. The dispersion relation of the anisotropy-driven whistler waves was measured by using the correlations among magnetic field data from four MMS satellites. The temperature anisotropy of energetic electrons is demonstrated with the 2D electron distribution function, which is unstable to the whistler wave generation. Moreover, the enhanced transport of electrons with a high parallel speed by the turbulence driven by the lower hybrid drift instability (LHDI) was suggested as the fundamental reason for the observed anisotropy. Although correlation between whistler and LHDI activities both in space and laboratory data provides circumstantial evidence for this hypothesis, further research is required to confirm the role of LHDI in the whistler wave excitation near the magnetospheric separatrix with an active X line.

Here, another MMS event with the similar whistler wave activity is analyzed and compared with the event reported by Yoo *et al.*[7] to have better insight into the role of LHDI in the whistler wave generation. In Sec. II, the overview of two MMS events with clear whistler wave activity is presented. In Sec. III, dispersion relations of the whistler mode are demonstrated. In Sec. IV, the measured electron distribution functions are shown, and it is verified that these distribution functions are unstable to the observed whistler mode by a linear analysis. Finally, in Sec. V, the possible role of LHDI in the whistler wave generation is discussed.

II. OVERVIEW OF TWO MMS EVENTS

High-resolution burst mode data from two MMS events are analyzed to understand excitation mechanisms and propagation characteristics of the whistler wave near the magnetospheric separatrix during asymmetric reconnection at the dayside magnetopause. The first one is a well-known MMS event where MMS encountered the electron diffusion region at the magnetopause on 16 October 2015.[9] The other event occurred on 19 September 2015, when MMS crossed the magnetopause near an active X line.[10] More details of these magnetopause events including the MMS trajectory can be found in the studies by Burch *et al.*[9] and Wang *et al.*[10] Whistler wave activity appeared near the magnetospheric separatrix about 10–15 d_i away from the X line for both events. Here, $d_i = c/\omega_{pi}$ is the ion skin depth and ω_{pi} is the ion (angular) plasma frequency.

Electron distribution functions are measured using a Fast Plasma Instrument (FPI).[11] The magnetic field is measured using a Search-Coil Magnetometer (SCM)[12] and a FluxGate Magnetometer (FGM),[13] while the electric field is measured using an Electric field Double Probe (EDP).[13]

The coordinate system in this study is *LMN*, with *L* along the reconnecting field component, *M* along the out-of-plane direction, and *N* normal to the current sheet. For the first event, we follow the transformation matrix given in the study by Burch *et al.*,[9] which transforms the geocentric-solar-ecliptic (GSE) coordinates to the *LMN* coordinates. For the second event, the matrix is obtained by a minimum variance analysis of the magnetic field during the current sheet crossing around 07:41:22 on 19 September 2015; the unit vector along *L*, *M*, and *N* is (0.244, 0.011, 0.970), (0.567, −0.813, −0.133), and (0.787, 0.582, −0.205) in GSE, respectively.

Figure 1 demonstrates the location where the whistler wave is observed by MMS. Both events occurred at the dayside magnetopause—the boundary between the magnetosphere (left side) and the magnetosheath (right side). Since plasma parameters and magnetic field strength in the magnetosphere are significantly different from those in the magnetosheath, the reconnection at the magnetopause is inherently asymmetric.[14] For example, the plasma density in the magnetopause (0.1–1 cm^{-3}) is one or two orders of magnitude smaller than the density in the magnetosheath (10–100 cm^{-3}). Due to this large density asymmetry, steep density gradients build up near the magnetospheric separatrix, leading to the development of LHDI-driven turbulence.[15–23] The LHDI-driven turbulence is characterized by strong, broadband electric field fluctuations whose energy is concentrated mostly below the lower hybrid frequency (f_{LH}).[15,16,19] This LHDI-driven turbulence obscures the location of the magnetospheric separatrix; the separatrix becomes an electron mixing region where some electrons from the exhaust region are transported to the magnetospheric side occasionally and vice versa.[22] As illustrated in Fig. 1 with a red circle, MMS spacecraft was in the electron mixing region (orange color) when it observed the whistler wave together with LHDI. The whistler wave disappears in the exhaust region (pink color).

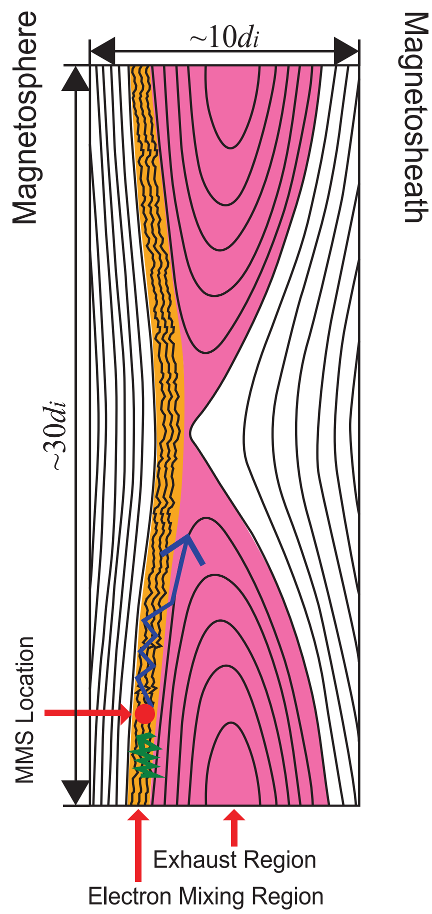

FIG. 1. Illustration of the MMS location when the whistler wave is observed. MMS satellites are in the electron mixing region (orange color), where electrons in the exhaust region (pink color) are transported by occasional LHDI activity. LHDI also transports magnetospheric electrons to the exhaust region. For both events presented here, MMS is 10–15 d_i away from the X line, as marked by a red circle. The path in the blue color represents a possible motion of energetic electrons with a dominant parallel velocity under the LHDI-driven turbulence. The path in the green color illustrates the guiding center motion of energetic electrons with a dominant perpendicular color. More discussion on these motions can be found in Sec. V.

A. Event on 16 October 2015

Figure 2(a) shows a power spectrogram of the magnetic field from a wavelet analysis. The magenta solid line indicates half of the local electron cyclotron frequency, $0.5f_{ce}$, while the black solid line represents the local lower hybrid frequency, f_{LH}. There is clear whistler wave activity near $0.5f_{ce}$ until MMS3 enters the exhaust region at 13:05:43, which is indicated by the red vertical dashed line. There are four features that suggest that MMS3 moves from the electron mixing region to the exhaust region. First, there is strong LHDI-driven turbulence, as shown in Figs. 2(a) and 2(c). This enhanced LHDI activity near the separatrix has been observed consistently during asymmetric magnetic reconnection.[15–23] Second, a sharp increase in the electron density exists, as shown in Fig. 2(d). Third, there is a decrease in the reconnecting magnetic field component, as presented in Fig. 2(e). Finally, the electron temperature decreases due to the increased

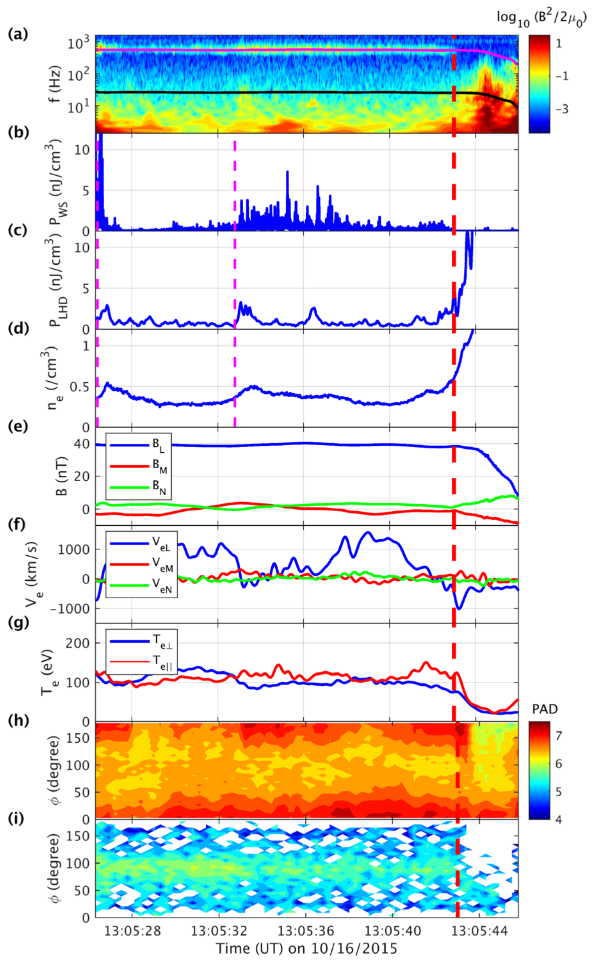

FIG. 2. Overview of an MMS event at the magnetopause on 16 October, 2015.[9] The red vertical dashed line in all panels indicates that the suggested time MMS3 enters the exhaust region. (a) Power spectrogram of the magnetic field measured by SCM. The magenta line denotes half of the local electron cyclotron frequency, $0.5f_{ce}$, while the black line indicates the lower hybrid frequency, f_{LH}. There is clear whistler wave activity near $0.5f_{ce}$ until MMS3 enters the exhaust region at 13:05:43. Time evolution of (b) power in the whistler mode (P_{WS}), (c) power in LHDI (P_{LHD}), and (d) electron density (n_e). Two magenta vertical dashed lines indicate the time where P_{WS}, P_{LHD}, and n_e start to increase. (e) Profile of the magnetic field measured by FGM. The decrease in B_L after 13:05:43 means that MMS3 enters the exhaust region. (f) Electron flow velocity ($\mathbf{V}_e$) profile measured by FPI. There is occasionally strong electron flow toward the X line (positive V_{eL}). (g) Electron temperature (T_e) profile. The blue line indicates the perpendicular electron temperature ($T_{e\perp}$), while the red line denotes the parallel electron temperature ($T_{e\parallel}$). Pitch angle distribution (PAD) of (h) middle-energy (200–2000 eV) and (i) high-energy (2–30 keV) electrons. The color bar shows the common logarithm of PAD, whose unit is eV/s cm^2 str eV (str stands for steradian). The PAD of middle-energy electrons shows anisotropy of $T_\parallel > T_\perp$, while that of high-energy electrons indicates the opposite temperature anisotropy ($T_\parallel < T_\perp$) in tail electrons.

population of the cold plasma in the exhaust that is from the cold magnetosheath. All these features occur around 13:05:43.

Figures 2(b)–2(d) show a time evolution of the power in the whistler wave, P_{WS} ($0.25f_{ce} < f < 0.75f_{ce}$), the power in LHD, P_{LHD} ($0.3f_{LH} < f < 1.4f_{LH}$), and electron density, n_e. As shown in Fig. 2(d), the local electron density starts to increase around 13:05:26.5 and 13:05:33, which is indicated by two magenta dashed lines. This density increase is caused by the transport of electrons from the exhaust region by LHDI.[22] This observation is supported by a simultaneous increase in low energy electron phase space density [Fig. 6(c)]. Furthermore, the correlation between P_{LHD} and n_e also supports the transport of magnetosheath electrons by LHDI; as shown in Figs. 2(c) and 2(d), the local density increase follows peaks in P_{LHD}. For reference, the unperturbed density of the magnetosphere for this event is about 0.3 cm^{-3}. The observation of cold electrons from the exhaust region with occasional LHDI activity provides convincing evidence that MMS3 was in the electron mixing region when it observed the whistler wave. The whistler wave activity also correlates with both P_{LHD} and n_e. As shown in Fig. 2(b), P_{WS} significantly increases right after P_{LHD} and n_e start to increase.

Figure 2(e) shows a time profile of the magnetic field, measured by FGM. Compared to B_L, both B_M and B_N components are negligible, which means that the guide field is negligible and MMS3 is not really far from the X line (estimated about $10d_i$ away).[9] The strength of B_L on the magnetosphere side is about 40 nT. The electron flow profile is shown in Fig. 2(f). It is worth noting that there is a sizable electron flow toward the X line (positive V_{eL}).

The electron temperature profile shown in Fig. 2(g) shows a general trend of $T_{e\parallel} > T_{e\perp}$ near the separatrix, which is due to the trapped particle dynamics with the acceleration potential.[24] Both parallel and perpendicular temperatures decrease significantly in the exhaust region where the electron population from the cold magnetosheath dominates.

Finally, the pitch angle distributions (PADs) of middle-energy (200–2000 eV) and high-energy (2–30 keV) electrons are shown in Figs. 2(h) and 2(i), respectively. For middle-energy electrons, electrons with a pitch angle ϕ close to 0° or 180° (parallel or antiparallel to the field line) are dominant over electrons with ϕ close to 90 (perpendicular to the field line), which means that $T_\perp < T_\parallel$ for these electrons. For high-energy electrons, on the other hand, PAD shows the opposite trend—electrons with ϕ close to 90 are dominant. This means that $T_{e\perp} > T_{e\parallel}$ for energetic electrons. This temperature anisotropy in tail electrons exists together with the whistler mode activity [Fig. 2(a)], until MMS3 enters the exhaust region at 13:05:43.

B. Event on 19 September 2015

Similar whistler activity is found in another MMS event on 19 September 2015. As shown in Fig. 3(a), the whistler mode around $f = 0.5f_{ce}$ is strong from 07:40:40 to 07:41:08. MMS4 enters the exhaust region around 07:41:08, which is supported by the increase in LHDI activity in Fig. 3(c), the large increase in the electron density n_e in Fig. 3(d), and the decrease in B_L in Fig. 3(e).

There is also an interesting correlation among P_{WS}, P_{LHD}, and n_e in this event. As shown in Figs. 3(a) and 3(c), there is an enhanced LHDI activity from 07:40:37 to 07:40:43. At the same time, the local electron density (n_e) increases significantly from about 0.2 cm^{-3} to 1 cm^{-3}, as shown in Fig. 3(d). In addition, there is a sharp decrease in T_e from about 200 eV to about 30 eV. Again, this is due to the LHDI-driven turbulent transport of cold electrons in the exhaust region to the magnetosphere side. Right after the intense LHDI activity, strong whistler wave activity starts, as shown in Figs. 3(a) and 3(b), which supports the causality between LHDI and the whistler mode.

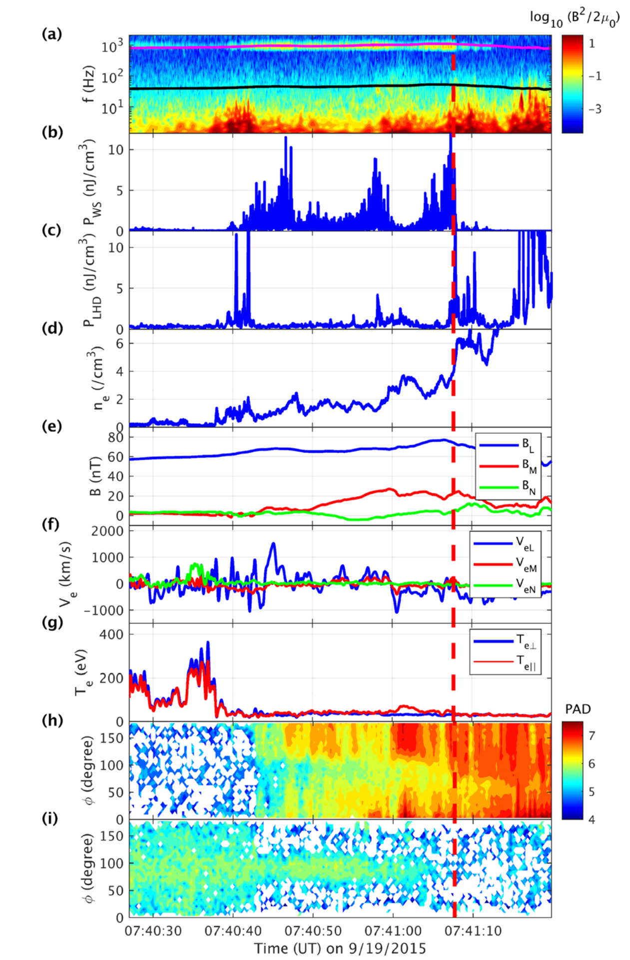

FIG. 3. Overview of an MMS event at the magnetopause on 19 September 2015.[10] The red vertical dashed line in all panels indicates that the suggested time MMS4 enters the exhaust region. (a) Power spectrogram of the magnetic field measured by SCM. The magenta line denotes half of the local electron cyclotron frequency, $0.5f_{ce}$, while the black line indicates the lower hybrid frequency, f_{LH}. Time evolution of (b) power in the whistler mode, (c) power in LHDI, and (d) electron density. For this event, strong whistler wave activity near $0.5f_{ce}$ starts right after intense LHDI activity around 07:40:40 and continues until MMS4 enters the exhaust region at 07:41:08. The local density increase coincides with the LHDI activity. (e) Profile of the magnetic field measured by FGM. B_L starts to decrease at 07:41:08, indicating that MMS4 enters the exhaust region. (f) Electron flow velocity ($\mathbf{V}_e$) profile measured by FPI. Unlike the previous event, there is no strong average electron flow. (g) Electron temperature (T_e) profile. The blue line indicates the perpendicular electron temperature, while the red line denotes the parallel electron temperature. Pitch angle distribution (PAD) of (h) middle-energy (200–2000 eV) and (i) high-energy (2–30 keV) electrons. Right after the intense LHDI activity, the PAD of middle-energy electrons shows anisotropy of $T_\parallel > T_\perp$, while that of high-energy electrons indicates the opposite temperature anisotropy ($T_\parallel < T_\perp$). The time period of the strong temperature anisotropy in high-energy electrons coincides with that of the strong whistler activity shown in (b).

The temperature anisotropy in energetic electrons, which is responsible for the whistler wave generation, also occurs right after the intense LHDI activity. As shown in Fig. 3(i), high-energy (2–30 keV) electrons have an isotropic PAD with a dominant population of electrons with $\phi°$–90°. It is important to see that the anisotropy is caused by a sudden "loss" of electrons with a dominant parallel velocity after the LHDI activity. This indicates that LHDI may be responsible for the loss of electrons with a dominant parallel velocity, which will be discussed in Sec. V. The temperature anisotropy of $T_\perp > T_\parallel$ in energetic electrons is the required condition for the anisotropy-driven whistler wave in this region.[7,25] This anisotropic PAD continues until MMS4 enters the exhaust region around 07:41:08. It is worth noting that the period where the anisotropic PAD exists coincides with the strong whistler wave activity. The LHDI activity and local density increase support that MMS4 was in the electron mixing region when it observed the whistler wave.

The middle-energy (200–2000 eV) electrons show the opposite PAD, where the phase space density of electrons with ϕ close to 0° or 180° is larger than that of electrons with ϕ close to 90°, as shown in Fig. 3(h). This means that the cold electrons from the exhaust region have been accelerated by the parallel electric field, which exists near the magnetospheric separatrix.[26]

III. MEASUREMENTS OF THE DISPERSION RELATION

The measurement of the dispersion relation is important for identifying the wave mode and understanding the wave propagation. It also provides important information on the wave excitation mechanism. Yoo *et al.*[7] provide the first clear measurement of the whistler wave dispersion near the reconnection site in space by using the maximum likelihood method.[27] The method requires correlations between data from each measurement point. Since the separation of MMS for the event on 16 October 2015, is about 10 km that is smaller than the wavelength of about 40 km, whistler wave signals from each MMS correlate with each other. Thus, the spectral power as a function of ω and $\mathbf{k}$, $P(\omega, \mathbf{k})$, from the maximum likelihood method demonstrates the wave dispersion, as shown in Fig. 4.

Figure 4(a) shows the maximum likelihood spectral power, $P(\omega, k_L)$ with $k_M = k_N = 0$. SCM data from 13:05:26.6 to 13:05:27 are used to obtain $P(\omega, \mathbf{k})$. As presented in Fig. 2(e), the magnetic field during the given time period has a dominating B_L component, such that k_L represents $k_\parallel$. The magenta dashed line indicates the cold plasma dispersion with $\theta = 0$, where θ is the angle between $\mathbf{k}$ and the magnetic field. The sold red line is the dispersion from a linear dispersion solver, WHAMP (waves in homogeneous, anisotropic, and multicomponent plasmas[28]), which agrees with the measured dispersion relation.

Figures 4(b) and 4(c) show $P(k_L, k_M)$ with $k_N = 0$ and $P(k_L, k_N)$ with $k_M = 0$ for ω = 3921 rad/s, respectively. The wave vector with the highest power at $\omega = 3921$ rad/s is $\mathbf{k} = (1.76, -0.16, -0.45) \times 10^{-4}$/m. In this case, θ is about 19°. Since MMS passed through the southern part of the X line structure,[9] the relatively small θ and positive k_L mean that whistler waves propagate toward the X line almost parallel to the magnetic field, which agrees with the previous research.[4] The phase velocity of the whistler mode is estimated to be about 2×10^7 m/s. The polarization of the wave from the singular value decomposition (SVD) analysis[29] is right-handed. The observed characteristics of the whistler wave such as the dominant $k_\parallel$ and high phase velocity are consistent with anisotropy-driven whistlers.[4,6,25]

For the event on 19 September 2015, the maximum likelihood method cannot be used, as the separation between spacecraft (∼100 km) is larger than the wavelength (∼30 km) of the whistler mode. In this case, two methods for single spacecraft data can be used

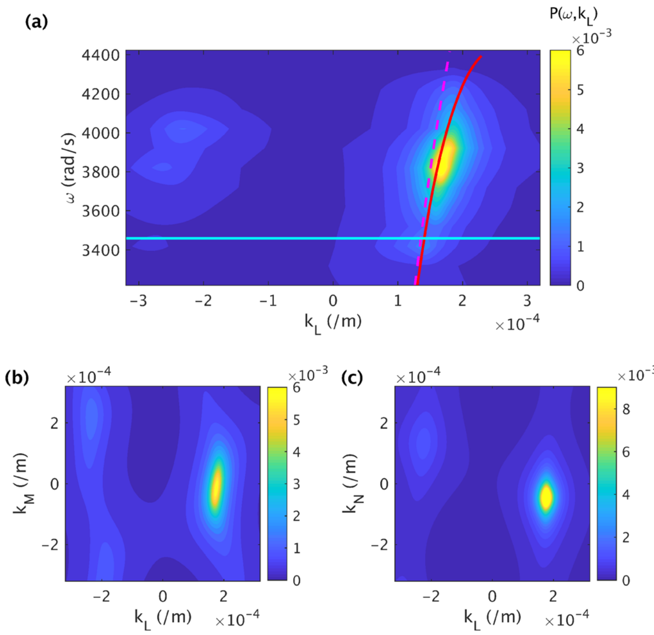

FIG. 4. Maximum likelihood power spectrum, $P(\omega, \mathbf{k})$ of the MMS magnetic field data from 13:05:26.6 to 13:05:27, demonstrating the dispersion relation of the whistler wave. (a) $P(\omega, k_L)$ with $k_M = k_N = 0$. Here, k_L represents $k_{\|}$. The horizontal cyan line indicates $0.5\omega_{ce}$ with $\omega_{ce} = 2\pi f_{ce}$. The magenta dashed line is the cold plasma dispersion relation of whistler waves with $\theta = 0$. The measured dispersion agrees with the red line, which is the dispersion relation calculated by WHAMP that includes effects from the electron temperature and flow velocity. (b) $P(k_L, k_M)$ with $\omega = 3921$ rad/s and $k_N = 0$. It peaks at $(k_L, k_M) = (1.75, -0.16) \times 10^{-4}$/m. (c) $P(k_L, k_N)$ with $\omega = 3921$ rad/s and $k_M = 0$. It peaks at $(k_L, k_N) = (1.76, -0.45) \times 10^{-4}$/m.

to obtain the dispersion relation. Both methods are based on Faraday's equation in the Fourier space, which is

$$\mathbf{k} \times \delta\mathbf{E}(\omega, \mathbf{k}) = \omega\delta\mathbf{B}(\omega, \mathbf{k}), \tag{1}$$

where $\delta\mathbf{E}(\omega, \mathbf{k})$ and $\delta\mathbf{B}(\omega, \mathbf{k})$ are the complex amplitude of the electric and magnetic field fluctuation in the Fourier space, respectively. In this study, $\delta\mathbf{E}(\omega, \mathbf{k})$ and $\delta\mathbf{B}(\omega, \mathbf{k})$ are obtained from the fast Fourier transform of EDP and SCM data, respectively. The main assumption of both methods is that there is one dominant wave mode for a given frequency. This means that the result is not reliable if there are multiple modes with a similar power for a frequency.

The first method is the SVD analysis by Santolík *et al.*[29] The basic idea of the SVD analysis is to create a real matrix equation equivalent to Eq. (1), which is solved by the singular value decomposition method to find the best estimate of the wave number vector $\mathbf{k}$. Here, the best estimate means a solution that minimizes errors from noise. The details on the SVD analysis can be found in the study by Santolík *et al.*[29]

The second method is based on the hodogram analysis, which is mathematically less rigorous than the SVD analysis. With the given $\delta\,\mathbf{B}$, the direction of $\mathbf{k}$ is determined from the condition $\mathbf{k} \cdot \Re(\delta\mathbf{B}) = 0$ and $\mathbf{k} \cdot \Im(\delta\mathbf{B}) = 0$, which is from Maxwell's equation $\nabla \cdot \mathbf{B} = 0$. Here, $\Re(\,)$ and $\Im(\,)$ mean the real and imaginary part of a complex quantity, respectively. Therefore, $\mathbf{k}$ is either parallel or antiparallel to the direction of $\Re(\delta\mathbf{B}) \times \Im(\delta\mathbf{B})$. This ambiguity can be removed by using the condition $\mathbf{k} \cdot \delta\mathbf{S} > 0$,[30] where $\delta\mathbf{S} = \Re(\delta\mathbf{E} \times \delta\mathbf{B})/\mu_0$ is the Poynting vector. This condition means that the phase velocity of a wave is generally close to the Poynting vector direction. Once the direction of $\mathbf{k}$ is determined, its magnitude can be obtained from the real part of Eq. (1).

Figure 5 shows the measured dispersion relations by both methods with MMS4 data from 07:40:46.5 to 07:40:47.5. These are power-

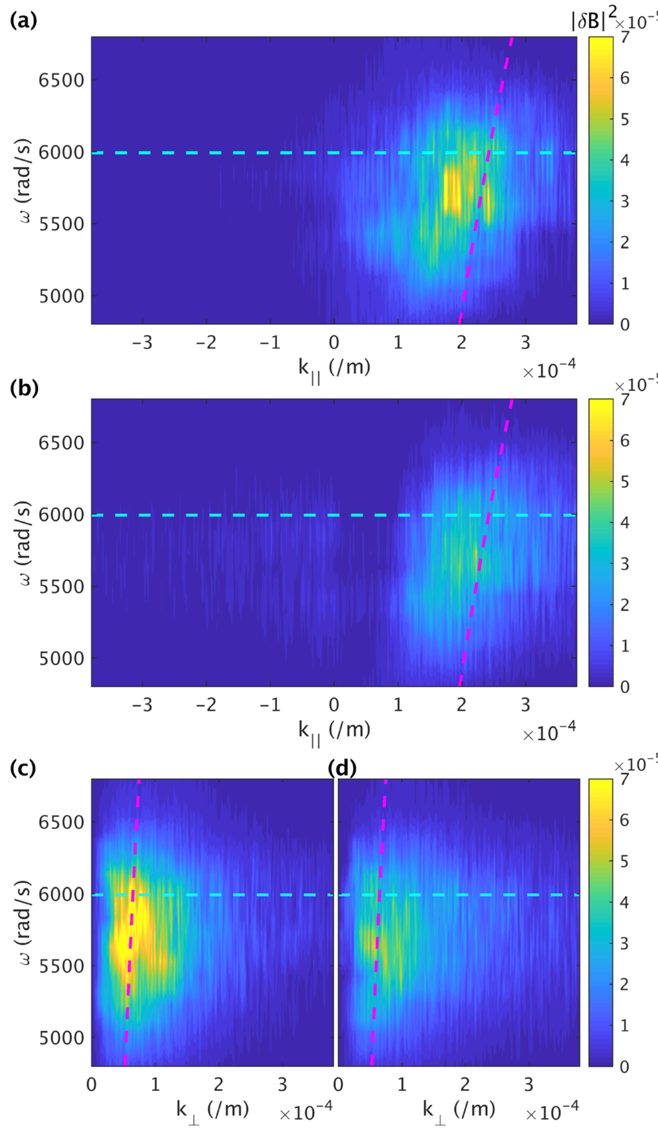

FIG. 5. Power-weighted ($|\delta\mathbf{B}|^2$) histogram to demonstrate the dispersion relation of the whistler wave. In all panels, the cyan dashed line indicates $0.5\omega_{ce}$, while the magenta dashed line denotes the dispersion relation of the whistler wave with $\theta = 15°$. Histogram of ω-$k_{\|}$ from (a) the singular value decomposition (SVD) analysis and (b) the histogram analysis. Histogram of ω-$k_{\perp}$ from (c) the singular value decomposition (SVD) analysis and (d) the histogram analysis. Both analyses show that $|k_{\|}| > k_{\perp}$ with $k_{\|} > 0$, which means that it propagates toward the X line almost parallel to the magnetic field. The measured dispersion relations generally underestimate $k_{\|}$, due to the violation of the major assumption of the unique $\mathbf{k}$ for a given ω and possibly due to errors in the electric field measurement.

weighted ($|\delta\mathbf{B}|^2$) histograms of ω and $k_\parallel$ or $k_\perp$. First, SCM data are partitioned into many segments with 512 data points. Then, the fast Fourier transform is conducted for each segment to obtain $\delta\mathbf{E}(\omega, \mathbf{k})$ and $\delta\mathbf{B}(\omega, \mathbf{k})$, which are used to obtain $\mathbf{k}(\omega)$ using the two methods. Each result is weighted by power in the magnetic field ($|\delta\mathbf{B}|^2$) and added up over every segment to generate histograms in Fig. 5.

Figures 5(a) and 5(c) show the dispersion relation from the SVD analysis. The magenta dashed line represents the cold plasma dispersion relation with $\theta = 15°$, $kd_e = \sqrt{\omega/(\omega_{ce}\cos\theta - \omega)}$, where $d_e = c/\omega_{pe}$ is the electron skin depth and ω_{ce} is the electron cyclotron frequency. The cyan dashed line indicates $0.5\omega_{ce}$. The measured dispersion relation shows $k_\parallel > k_\perp$ and is in relatively good agreement with the cold plasma dispersion relation. However, the SVD analysis generally underestimates $k_\parallel$, which is mostly caused by the violation of the assumption of a unique $\mathbf{k}$ for a given ω and possibly by the errors in the electric field measurements.

Figures 5(b) and 5(d) show the dispersion relation from the hodogram analysis, which is similar to that from the SVD analysis. The main difference is that the SVD analysis has smaller variance in the power distribution; histograms from the SVD analysis show a higher power concentration near the average value of k. This means that the average result is the same for both methods, but the SVD analysis, which is mathematically more rigorous, requires a lower number of segments to identify the dispersion relation. The hodogram analysis, on the other hand, is simpler and faster.

The measured dispersion relation for the second MMS event also shows similar features of the whistler mode in the first event; $k_\parallel > k_\perp$, positive $k_\parallel$ (propagating toward the X line), and the phase velocity ($\sim 3 \times 10^7$ m/s) exceeding the electron thermal velocity. This agreement proves that the whistler wave is excited by the same mechanism for both events—temperature anisotropy in tail electrons.

IV. ELECTRON DISTRIBUTION FUNCTION

For better understanding of the whistler wave generation mechanism, the 2D electron distribution function during the same time period of the dispersion relation measurement is presented in Fig. 6(a). The measured distribution function shows interesting temperature anisotropy, which depends on the electron energy. The black dashed semicircles indicate the sample contours with an isotropic electron distribution function. For electrons with a low speed ($v_e < 3v_{the}$; v_e is the electron speed; $v_{the} \sim 4 \times 10^6$ m/s), contours of the phase space density (f_e) are elongated along the parallel direction, indicating $T_\parallel > T_\perp$ for these electrons. This anisotropy is consistent with trapped particle dynamics under an acceleration potential.[24] The magenta dashed lines denote the boundaries between trapped and passing electrons, based on the anticipated acceleration potential and magnitude of the magnetic field far from the reconnection region; electrons between the lines are trapped due to the parallel electric field and magnetic mirror force. For tail electrons ($v_e > 3v_{the}$), however, the trend is reversed; contours are elongated along the perpendicular direction. These tail electrons with $T_\perp > T_\parallel$ excite the whistler mode.[25,31]

To confirm this argument, WHAMP has been employed to obtain the dispersion relation and the growth rate. Due to the constraint in the solver, the local 2D electron distribution function must be modeled as a sum of bi-Maxwellian distribution functions. Figure 6(b) shows the modeled electron distribution function, which has the same key features as the measured distribution function. The

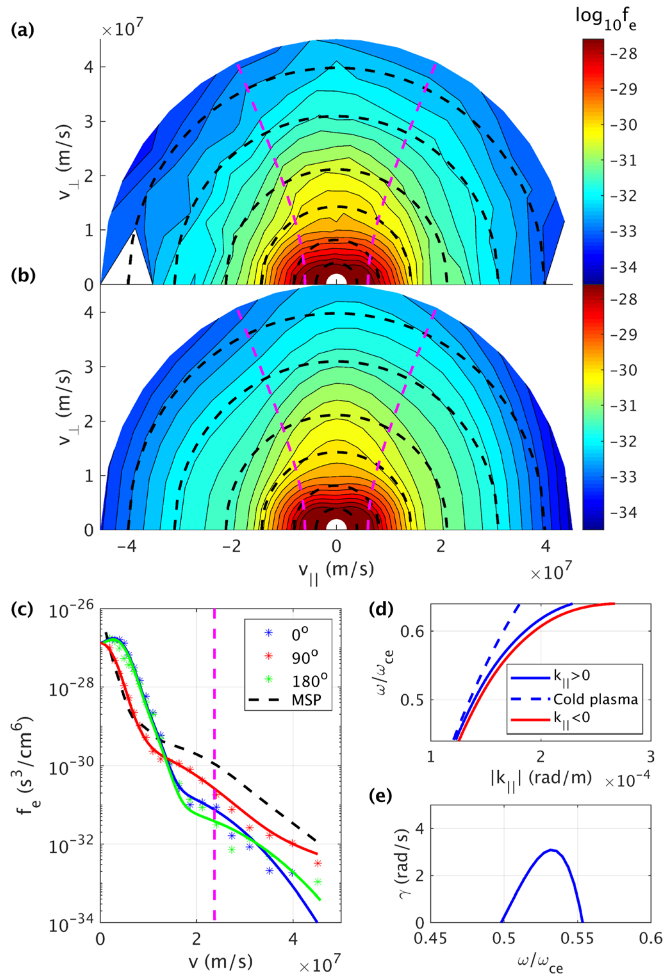

FIG. 6. (a) 2D electron distribution function [$f_e(v_\parallel, v_\perp)$] measured by MMS3 from 13:05:26.5 to 13:05:27 on 16 October, 2015. Black dashed semicircles represent the sample contours of an isotropic f_e. Magenta dashed lines indicate the boundaries between trapped and passing electrons. (b) Modeled 2D electron distribution function for the WHAMP analysis. (c) 1D distribution functions for $\phi = 0°$ (blue), 90° (red), and 180° (green), where ϕ is the pitch angle. Solid lines are the results from the modeling. The black dashed line is a reference distribution function averaged over the pitch angle further away from the separatrix region in Fig. 7. The magenta dashed line denotes the resonance velocity for $\omega \sim 0.55\omega_{ce}$. (d) Calculated dispersion relation with $\theta = 0$. The blue sold line is the dispersion for $k_\parallel > 0$ (toward X line) calculated by WHAMP, while the red sold line is that for $k_\parallel < 0$. The difference between two solid lines is caused by the electron flow ($\sim$270 km/s) toward the X line. The blue dashed line indicates the dispersion in a cold plasma. The discrepancy between two blue lines results from the electron temperature. (e) Growth rate calculated by WHAMP.

combined electron density and parallel flow velocity ($\sim$270 km/s) also match with the measured values.

Figure 6(d) shows the dispersion relation computed by WHAMP for $k_\parallel > 0$ (blue solid line) and for $k_\parallel < 0$ (red solid line). Two lines are slightly different, which is caused by the effect from the local electron flow (positive V_{eL}). The blue dashed line indicates the dispersion relation in a cold plasma, which is different from the blue solid line especially for $\omega > 0.5\omega_{ce}$. This discrepancy is mostly due to effects from thermal and energetic electrons.

Figure 6(e) shows the growth rate (γ) for $\theta = 0$ computed by WHAMP. WHAMP expects a positive growth rate for $0.5\omega_{ce} \lesssim \omega \lesssim 0.6\omega_{ce}$ for $k_\parallel > 0$, which agrees with measurements. The whistler mode with $k_\parallel < 0$, on the other hand, is marginally stable ($\gamma \lesssim 0$, not shown) due to the larger phase space density of resonant electrons with $|v_\parallel| \gg v_\perp$.

To understand the difference, it is important to understand the interaction of the wave with resonant electrons. The electrons are resonant with the wave when its parallel velocity satisfies the following cyclotron resonance condition: $\omega - v_\parallel k_\parallel = \omega_{ce}$. In other words, the resonance occurs when the Doppler-shifted frequency of the wave is the same as electron cyclotron frequency. This resonant condition indicates that the whistler mode with $k_\parallel < 0$ is resonant with electrons with a positive parallel velocity, since $\omega = 0.5\omega_{ce}$, while the mode with $k_\parallel > 0$ is resonant with electrons with a negative parallel velocity. Resonant electrons with a dominant parallel velocity ($|v_\parallel| \gg v_\perp$) damp the whistler wave, while resonant electrons with a dominant perpendicular velocity ($v_\perp \gg |v_\parallel|$) excite the whistler wave.

Figure 6(c) clearly shows that the phase space density of electrons with resonant velocity ($|V_{res}| \approx 2$–3×10^7 m/s) with $\phi = 0$ (blue asterisks, resonant with whistlers with $k_\parallel < 0$) is higher than that with $\phi = 180°$ (green asterisks, resonant with whistlers with $k_\parallel > 0$).

There is a shoulder near the phase velocity of whistlers ($\sim 2 \times 10^7$ m/s) in $f_e(\phi = 0°)$ [blue line in Fig. 6(c)], which has been observed together with whistler waves.[5,6] It should be mentioned that this shoulder structure is not an electron beam exciting the whistler mode. As mentioned earlier, these electrons are resonant with the whistler mode with $k_\parallel < 0$, not the mode with $k_\parallel > 0$. The reason why these electrons have a parallel velocity similar to the phase velocity of whistlers with $k_\parallel > 0$ is that the wave frequency is $0.5\omega_{ce}$. Since the whistler wave with $k_\parallel < 0$ is marginally stable, it is more reasonable to say that the shoulder structure results from damping of waves: WHAMP calculations without the shoulder structure show that the growth rate of the whistler waves with $k_\parallel < 0$ becomes positive. This shoulder structure leads to the aforementioned larger phase space density of resonant electrons with $|v_\parallel| \gg v_\perp$, making the whistler mode with $k_\parallel < 0$ marginally stable.

For reference, the electron distribution function in the magnetosphere away from the reconnection region has been examined. It is measured by MMS3 from UT10:56:00 to 10:56:02 on 16 October 2015. Near this time, there are minimal changes over time in the magnetic field, electron density, and electron velocity. As an example, the electron density profile is shown in Fig. 7(a). The electron density remains around 0.3 cm^{-3}, indicating that MMS is away from the reconnection region or the magnetospheric separatrix where LHDI creates rapid changes in the density, as shown in both Figs. 2(d) and 3(d).

In this region, the 2D distribution function is much more isotropic, as shown in Fig. 7(b). A WHAMP analysis shows that it is also marginally stable to the whistler mode. There is a possibility that the loss of energetic electrons with a high parallel velocity along the open magnetic field line in the magnetosphere excites whistler waves. However, if there is no fast change in the magnetic geometry, the wave particle interaction makes the distribution function marginally stable to the wave mode. The shoulder structure around $v \sim 9 \times 10^6$ m/s for both $\phi = 0$ and 180 in Fig. 7(b) is evidence of the interaction between

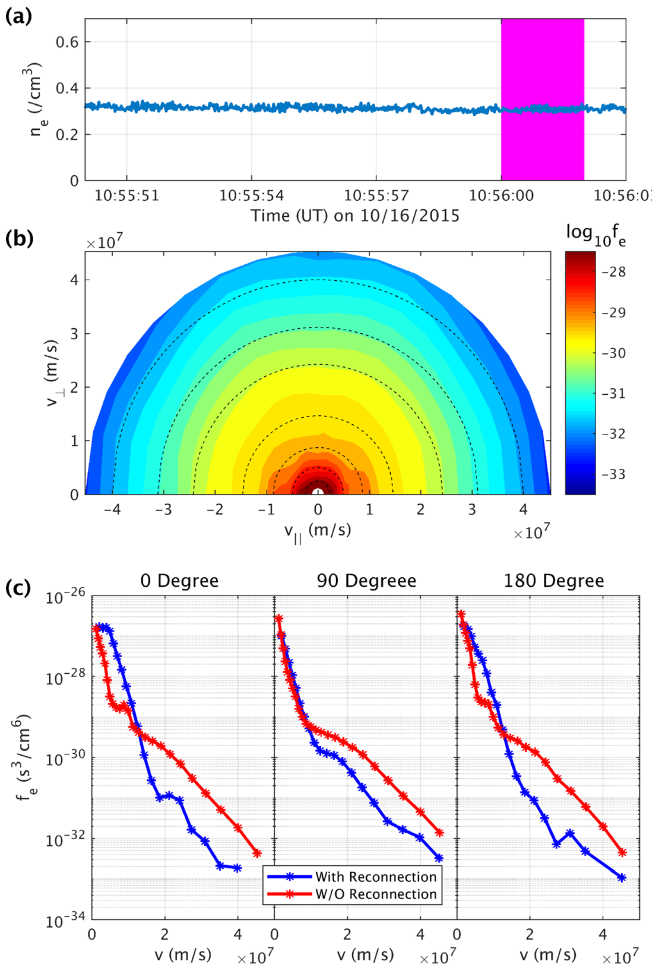

FIG. 7. (a) Electron density profile in the magnetosphere much away from the reconnection region, measured by MMS3 on 16 October, 2015. As there is no effect from LHDI in this region, the density is steady. (b) 2D electron distribution function in the magnetosphere. The magenta box in (a) indicates the time where the 2D electron distribution function is obtained. Compared to that near the magnetospheric separatrix, the distribution function is fairly isotropic. (c) 1D electron distribution functions for $\phi = 0°$, 90°, and 180°, where ϕ is the pitch angle. Blue lines are from data near the magnetospheric separatrix [the same as in Fig. 6(c)], while the red lines are from the identical data for (b).

the whistler mode and electrons. The small temperature anisotropy in the electron tail excites the whistler wave whose phase velocity parallel to the field is about 9×10^6 m/s. Then, it is damped by resonance electrons, creating a shoulder structure and making the whistler mode marginally stable. This means that the loss cone distribution by the open field line in the magnetosphere is not responsible for the whistler wave excitation near the separatrix region; we need fast dynamic changes in the magnetic field topology, associated with magnetic reconnection.

Compared to the distribution functions in the magnetosphere [red lines in Fig. 7(c)], those near the magnetospheric separatrix [blue lines in Fig. 7(c)] show that there is a significant reduction in the phase space density of energetic electrons with $\phi \sim 0$ and $\phi \sim 180°$. As mentioned before, this loss of electrons with a dominant parallel velocity is responsible for the whistler wave generation. This change in the phase space density of electrons mostly parallel or antiparallel to the field line cannot be explained by the trapped particle dynamics[24] that only expects the reduction of the phase space density with $\phi \sim 90°$. In Sec. V, the possible role of the turbulent transport by LHDI in the loss of energetic electrons with a dominant parallel velocity is discussed. As mentioned in Sec. II, the increase in the phase space density for lower energy electrons near the magnetospheric separatrix is caused by electrons from the exhaust region which are transported by LHDI-driven turbulence.[22]

V. DISCUSSION AND SUMMARY

The correlated behavior between activities of LHDI and the whistler mode in both events suggests that LHDI may lead to the dynamic change in the electron distribution function. The local electron density increase followed by the LHDI activity in Figs. 2 and 3 prove that LHDI initiates the electron mixing process near the magnetospheric separatrix.[22] On the other hand, Fig. 3(i) suggests that LHDI produces a preferential loss of electrons with a high parallel velocity, causing the temperature anisotropy in tail electrons which excites the observed whistler wave.

The turbulent transport process by LHDI is caused by the $\mathbf{E} \times \mathbf{B}$ motion from strong fluctuations in the electric field.[22] The magnitude of electric field fluctuations by LHDI exceeds that of the reconnection electric field,[15,17,19,21] which means that the particle drift motion near the magnetospheric separatrix is dominated by the strong electric field fluctuation. This $\mathbf{E} \times \mathbf{B}$ drift motion does not depend on the parallel velocity. Thus, to understand the difference, more detailed analysis on the particle motion is required.

The key difference between electrons with a dominant parallel velocity and those with a dominant perpendicular velocity is the ability to move into the exhaust region by a velocity kick from the turbulent electric field fluctuation. When electrons with a high parallel velocity see the magnetic field in the exhaust region by a kick from LHDI, they travel quickly along the magnetic field in the exhaust region and do not come back to the magnetosphere side. An example motion for this group of electrons is illustrated by a blue path in Fig. 1. However, electrons with a dominant perpendicular velocity can remain in the mixing zone longer due to their large gyro radius, moving back and forth by the fluctuating electric field. An example of the guiding center motion for this group of electrons is illustrated by a green line in Fig. 1. This picture can explain the sudden change in PAD of energetic electrons right after the intense LHDI activity, as presented in Fig. 3(i). This argument can be verified by running test particles near the magnetospheric separatrix under the LHDI-driven turbulence, which is a potential future research topic.

It should be mentioned that the exact mechanism for the observed anisotropy in tail electrons requires further investigation. Besides LHDI, there is a possibility that the observed 2D electron distribution is explained by a model based on the double adiabatic theory.[32] The measurement location is away from the X line, such that there is no significant change in the local magnetic field strength during the whistler wave activity; the local flux tube has not been expanded. The part of the flux tube, on the other hand, may be stretched as the tube approaches the X-line, resulting in the decrease in the average density in the flux tube. In this case, the electrons with a high parallel velocity can be dominantly cooled. However, this mechanism cannot explain the increase in the local electron density observed around UT13:05:27, which is caused by the low-energy electrons from the magnetosheath. The density increase indicates that the part of the flux tube has been already affected by the electron mixing process via LHID-driven turbulence.[22]

In summary, two MMS reconnection events at the dayside magnetopause with whistler wave activity near $0.5f_{ce}$ are analyzed. The whistler wave exists in the electron mixing region near the magnetospheric separatrix. In both events, the correlation between LHDI and the whistler mode is observed. The anisotropy in energetic electrons is caused by the loss of tail electrons with a dominant parallel velocity. This anisotropy in the tail electrons results in the excitation of the observed whistler mode. The measured dispersion relations of the whistler mode show that the whistler wave propagates toward the X line mostly parallel to the magnetic field ($\theta < 20°$). The 2D electron distribution function demonstrates the temperature anisotropy in low energy electrons ($T_\parallel > T_\perp$) as well as that in high-energy electrons ($T_\parallel < T_\perp$). A linear analysis verifies that the observed 2D distribution is unstable to the whistler mode. Finally, a possible explanation of the observed temperature anisotropy by the preferential loss of electrons with a high parallel velocity due to the turbulent transport process by LHDI is proposed.

This whistler wave around $0.5f_{ce}$ shows that there is an active X line nearby. Moreover, the whistler mode can help determine the location of spacecraft because it is an important indicator of the electron mixing region near the magnetospheric separatrix. The impact of the whistler wave on magnetic reconnection requires further investigation, as current research is limited to the wave near the magnetospheric separatrix. Because the whistler mode can also be excited near the X line,[8] it is important to study the excitation mechanism near the X line and to address possible role of the whistler wave in magnetic reconnection.

ACKNOWLEDGMENTS

This work was supported by Contract No. DE-AC0209CH11466, NSF Grant Nos. AGS-1619584 and AGS-1552142, DOE Grant No. DESC0016278, and NASA Grant Nos. 80NSSC18K1369 and 80NSSC17K0012. All MMS data used for this study are available at https://lasp.colorado.edu/mms/sdc/public/. The authors thank Ms. H. Kim for her contributions.

REFERENCES

[1] E. G. Zweibel and M. Yamada, "Magnetic reconnection in astrophysical and laboratory plasmas," Annu. Rev. Astron. Astrophys. **47**, 291–332 (2009).
[2] M. Yamada, R. Kulsrud, and H. Ji, "Magnetic reconnection," Rev. Mod. Phys. **82**, 603–664 (2010).
[3] A. Vaivads, Y. Khotyaintsev, M. André, and R. Treumann, "Plasma waves near reconnection sites," in *Geospace Electromagnetic Waves and Radiation*, edited by J. W. LaBelle and R. A. Treumann (Springer Berlin Heidelberg, Berlin, Heidelberg, 2006), pp. 251–269.
[4] O. Le Contel, A. Retinó, H. Breuillard, L. Mirioni, P. Robert, A. Chasapis, B. Lavraud, T. Chust, L. Rezeau, F. D. Wilder, D. B. Graham, M. R. Argall, D. J. Gershman, P.-A. Lindqvist, Y. V. Khotyaintsev, G. Marklund, R. E. Ergun, K. A. Goodrich, J. L. Burch, R. B. Torbert, J. Needell, M. Chutter, D. Rau, I. Dors, C. T. Russell, W. Magnes, R. J. Strangeway, K. R. Bromund, H. K. Leinweber, F. Plaschke, D. Fischer, B. J. Anderson, G. Le, T. E. Moore, C. J. Pollock, B. L. Giles, J. C. Dorelli, L. Avanov, and Y. Saito, "Whistler mode waves and hall fields detected by mms during a dayside magnetopause crossing," Geophys. Res. Lett. **43**, 5943–5952, https://doi.org/10.1002/2016GL068968 (2016).

[5]F. D. Wilder, R. E. Ergun, K. A. Goodrich, M. V. Goldman, D. L. Newman, D. M. Malaspina, A. N. Jaynes, S. J. Schwartz, K. J. Trattner, J. L. Burch, M. R. Argall, R. B. Torbert, P.-A. Lindqvist, G. Marklund, O. Le Contel, L. Mirioni, Y. V. Khotyaintsev, R. J. Strangeway, C. T. Russell, C. J. Pollock, B. L. Giles, F. Plaschke, W. Magnes, S. Eriksson, J. E. Stawarz, A. P. Sturner, and J. C. Holmes, "Observations of whistler mode waves with nonlinear parallel electric fields near the dayside magnetic reconnection separatrix by the magnetospheric multiscale mission," Geophys. Res. Lett. **43**, 5909–5917, https://doi.org/10.1002/2016GL069473 (2016).

[6]F. D. Wilder, R. E. Ergun, D. L. Newman, K. A. Goodrich, K. J. Trattner, M. V. Goldman, S. Eriksson, A. N. Jaynes, T. Leonard, D. M. Malaspina, N. Ahmadi, S. J. Schwartz, J. L. Burch, R. B. Torbert, M. R. Argall, B. L. Giles, T. D. Phan, O. Le Contel, D. B. Graham, Y. V. Khotyaintsev, R. J. Strangeway, C. T. Russell, W. Magnes, F. Plaschke, and P.-A. Lindqvist, "The nonlinear behavior of whistler waves at the reconnecting dayside magnetopause as observed by the magnetospheric multiscale mission: A case study," J. Geophys. Res. **122**, 5487–5501, https://doi.org/10.1002/2017JA024062 (2017).

[7]J. Yoo, J. Jara-Almonte, E. Yerger, S. Wang, T. Qian, A. Le, H. Ji, M. Yamada, W. Fox, E.-H. Kim, L.-J. Chen, and D. J. Gershman, "Whistler wave generation by anisotropic tail electrons during asymmetric magnetic reconnection in space and laboratory," Geophys. Res. Lett. **45**, 8054–8061, https://doi.org/10.1029/2018GL079278 (2018).

[8]D. Cao, H. S. Fu, J. B. Cao, T. Y. Wang, D. B. Graham, Z. Z. Chen, F. Z. Peng, S. Y. Huang, Y. V. Khotyaintsev, M. André, C. T. Russell, B. L. Giles, P.-A. Lindqvist, R. B. Torbert, R. E. Ergun, O. Le Contel, and J. L. Burch, "MMS observations of whistler waves in electron diffusion region," Geophys. Res. Lett. **44**, 3954–3962, https://doi.org/10.1002/2017GL072703 (2017).

[9]J. L. Burch, R. B. Torbert, T. D. Phan, L.-J. Chen, T. E. Moore, R. E. Ergun, J. P. Eastwood, D. J. Gershman, P. A. Cassak, M. R. Argall, S. Wang, M. Hesse, C. J. Pollock, B. L. Giles, R. Nakamura, B. H. Mauk, S. A. Fuselier, C. T. Russell, R. J. Strangeway, J. F. Drake, M. A. Shay, Y. V. Khotyaintsev, P.-A. Lindqvist, G. Marklund, F. D. Wilder, D. T. Young, K. Torkar, J. Goldstein, J. C. Dorelli, L. A. Avanov, M. Oka, D. N. Baker, A. N. Jaynes, K. A. Goodrich, I. J. Cohen, D. L. Turner, J. F. Fennell, J. B. Blake, J. Clemmons, M. Goldman, D. Newman, S. M. Petrinec, K. J. Trattner, B. Lavraud, P. H. Reiff, W. Baumjohann, W. Magnes, M. Steller, W. Lewis, Y. Saito, V. Coffey, and M. Chandler, "Electron-scale measurements of magnetic reconnection in space," Science **352**, aaf2939 (2016).

[10]S. Wang, L.-Â. Chen, M. Hesse, D. J. Gershman, J. Dorelli, B. Giles, R. B. Torbert, C. J. Pollock, B. Lavraud, R. Strangeway, R. E. Ergun, J. Burch, L. Avanov, T. E. Moore, and Y. Saito, "Ion demagnetization in the magnetopause current layer observed by MMS," Geophys. Res. Lett. **43**, 4850–4857, https://doi.org/10.1002/2016GL069406 (2016).

[11]C. Pollock, T. Moore, A. Jacques, J. Burch, U. Gliese, Y. Saito, T. Omoto, L. Avanov, A. Barrie, V. Coffey, J. Dorelli, D. Gershman, B. Giles, T. Rosnack, C. Salo, S. Yokota, M. Adrian, C. Aoustin, C. Auletti, S. Aung, V. Bigio, N. Cao, M. Chandler, D. Chornay, K. Christian, G. Clark, G. Collinson, T. Corris, A. De Los Santos, R. Devlin, T. Diaz, T. Dickerson, C. Dickson, A. Diekmann, F. Diggs, C. Duncan, A. Figueroa-Vinas, C. Firman, M. Freeman, N. Galassi, K. Garcia, G. Goodhart, D. Guererro, J. Hageman, J. Hanley, E. Hemminger, M. Holland, M. Hutchins, T. James, W. Jones, S. Kreisler, J. Kujawski, V. Lavu, J. Lobell, E. LeCompte, A. Lukemire, E. MacDonald, A. Mariano, T. Mukai, K. Narayanan, Q. Nguyan, M. Onizuka, W. Paterson, S. Persyn, B. Piepgrass, F. Cheney, A. Rager, T. Raghuram, A. Ramil, L. Reichenthal, H. Rodriguez, J. Rouzaud, A. Rucker, Y. Saito, M. Samara, J.-A. Sauvaud, D. Schuster, M. Shappirio, K. Shelton, D. Sher, D. Smith, K. Smith, S. Smith, D. Steinfeld, R. Szymkiewicz, K. Tanimoto, J. Taylor, C. Tucker, K. Tull, A. Uhl, J. Vloet, P. Walpole, S. Weidner, D. White, G. Winkert, P.-S. Yeh, and M. Zeuch, "Fast plasma investigation for magnetospheric multiscale," Space Sci. Rev. **199**, 331–406 (2016).

[12]O. Le Contel, P. Leroy, A. Roux, C. Coillot, D. Alison, A. Bouabdellah, L. Mirioni, L. Meslier, A. Galic, M. C. Vassal, R. B. Torbert, J. Needell, D. Rau, I. Dors, R. E. Ergun, J. Westfall, D. Summers, J. Wallace, W. Magnes, A. Valavanoglou, G. Olsson, M. Chutter, J. Macri, S. Myers, S. Turco, J. Nolin, D. Bodet, K. Rowe, M. Tanguy, and B. de la Porte, "The search-coil magnetometer for MMS," Space Sci. Rev. **199**, 257–282 (2016).

[13]R. B. Torbert, C. T. Russell, W. Magnes, R. E. Ergun, P.-A. Lindqvist, O. LeContel, H. Vaith, J. Macri, S. Myers, D. Rau, J. Needell, B. King, M. Granoff, M. Chutter, I. Dors, G. Olsson, Y. V. Khotyaintsev, A. Eriksson, C. A. Kletzing, S. Bounds, B. Anderson, W. Baumjohann, M. Steller, K. Bromund, G. Le, R. Nakamura, R. J. Strangeway, H. K. Leinweber, S. Tucker, J. Westfall, D. Fischer, F. Plaschke, J. Porter, and K. Lappalainen, "The fields instrument suite on MMS: Scientific objectives, measurements, and data products," Space Sci. Rev. **199**, 105–135 (2016).

[14]F. S. Mozer and P. L. Pritchett, "Electron physics of asymmetric magnetic field reconnection," Space Sci. Rev. **158**, 119–143 (2011).

[15]F. S. Mozer, M. Wilber, and J. F. Drake, "Wave associated anomalous drag during magnetic field reconnection," Phys. Plasmas **18**, 102902 (2011).

[16]P. L. Pritchett, F. S. Mozer, and M. Wilber, "Intense perpendicular electric fields associated with three-dimensional magnetic reconnection at the subsolar magnetopause," J. Geophys. Res. **117**, A06212, https://doi.org/10.1029/2012JA017533 (2012).

[17]V. Roytershteyn, W. Daughton, H. Karimabadi, and F. S. Mozer, "Influence of the lower-hybrid drift instability on magnetic reconnection in asymmetric configurations," Phys. Rev. Lett. **108**, 185001 (2012).

[18]D. B. Graham, Y. V. Khotyaintsev, A. Vaivads, M. André, and A. N. Fazakerley, "Electron dynamics in the diffusion region of an asymmetric magnetic reconnection," Phys. Rev. Lett. **112**, 215004 (2014).

[19]J. Yoo, M. Yamada, H. Ji, J. Jara-Almonte, C. E. Myers, and L.-J. Chen, "Laboratory study of magnetic reconnection with a density asymmetry across the current sheet," Phys. Rev. Lett. **113**, 095002 (2014).

[20]L. Price, M. Swisdak, J. F. Drake, P. A. Cassak, J. T. Dahlin, and R. E. Ergun, "The effects of turbulence on three-dimensional magnetic reconnection at the magnetopause," Geophys. Res. Lett. **43**, 6020–6027, https://doi.org/10.1002/2016GL069578 (2016).

[21]J. Yoo, B. Na, J. Jara-Almonte, M. Yamada, H. Ji, V. Roytershteyn, M. R. Argall, W. Fox, and L.-J. Chen, "Electron heating and energy inventory during asymmetric reconnection in a laboratory plasma," J. Geophys. Res. **122**, 9264–9281, https://doi.org/10.1002/2017JA024152 (2017).

[22]A. Le, W. Daughton, L.-J. Chen, and J. Egedal, "Enhanced electron mixing and heating in 3-d asymmetric reconnection at the earth's magnetopause," Geophys. Res. Lett. **44**, 2096–2104, https://doi.org/10.1002/2017GL072522 (2017).

[23]D. B. Graham, Y. V. Khotyaintsev, C. Norgren, A. Vaivads, M. André, S. Toledo-Redondo, P.-A. Lindqvist, G. T. Marklund, R. E. Ergun, W. R. Paterson, D. J. Gershman, B. L. Giles, C. J. Pollock, J. C. Dorelli, L. A. Avanov, B. Lavraud, Y. Saito, W. Magnes, C. T. Russell, R. J. Strangeway, R. B. Torbert, and J. L. Burch, "Lower hybrid waves in the ion diffusion and magnetospheric inflow regions," J. Geophys. Res. **122**, 517–533, https://doi.org/10.1002/2016JA023572 (2017).

[24]J. Egedal, W. Fox, N. Katz, M. Porkolab, M. ØÂieroset, R. P. Lin, W. Daughton, and J. F. Drake, "Evidence and theory for trapped electrons in guide field magnetotail reconnection," J. Geophys. Res. **113**, A12207, https://doi.org/10.1029/2008JA013520 (2008).

[25]C. F. Kennel and H. E. Petschek, "Limit on stably trapped particle fluxes," J. Geophys. Res. **71**, 1–28, https://doi.org/10.1029/JZ071i001p00001 (1966).

[26]J. Egedal, W. Daughton, and A. Le, "Large-scale electron acceleration by parallel electric fields during magnetic reconnection," Nat. Phys. **8**, 321–324 (2012).

[27]J. Capon, "High-resolution frequency-wavenumber spectrum analysis," Proc. IEEE **57**, 1408–1418 (1969).

[28]K. Rönnmark, *Waves in Homogeneous, Anisotropic, Multicomponent Plasmas, Technical Report* (Kiruna Geophysics Institute, Kiruna, Sweden, 1982).

[29]O. Santolík, M. Parrot, and F. Lefeuvre, "Singular value decomposition methods for wave propagation analysis," Radio Sci. **38**, 1010, https://doi.org/10.1029/2000RS002523 (2003).

[30]U. Taubenschuss, Y. V. Khotyaintsev, O. Santolík, A. Vaivads, C. M. Cully, O. L. Contel, and V. Angelopoulos, "Wave normal angles of whistler mode chorus rising and falling tones," J. Geophys. Res.: Space Phys. **119**, 9567–9578, https://doi.org/10.1002/2014JA020575 (2014).

[31]S. P. Gary and J. Wang, "Whistler instability: Electron anisotropy upper bound," J. Geophys. Res. **101**, 10749–10754, https://doi.org/10.1029/96JA00323 (1996).

[32]P. Montag, J. Egedal, E. Lichko, and B. Wetherton, "Impact of compressibility and a guide field on fermi acceleration during magnetic island coalescence," Phys. Plasmas **24**, 062906 (2017).